Deep-Sea Research, 1971, Vol. 18, pp. 145 to 165. Pergamon Press. Printed in Great Britain.

# Water masses and circulation patterns in the region of the Blake–Bahama Outer Ridge*

ANTHONY F. AMOS,† ARNOLD L. GORDON† and ERIC D. SCHNEIDER‡

(*Received* 26 *January* 1970; *in revised form* 21 *August* 1970; *accepted* 28 *August* 1970)

**Abstract**—The water masses and circulation patterns of the Blake–Bahama Outer Ridge area of the western North Atlantic were studied using a salinity/temperature/depth (STD) recording system. The dynamic method was applied to STD data in the deep ocean, revealing that the Western Boundary Undercurrent (WBUC) flows with velocities up to 26 cm $sec^{-1}$ at the bottom on the eastern flank of the Outer Ridge. The volume transport was computed to be $22 \times 10^6$ $m^3$/sec. The high Antarctic Bottom Water (AABW) content (up to 20%) of this current suggests that AABW flowing north into the western North Atlantic Basin is deflected by the ocean basin hills, at about 35°N merges with North Atlantic Deep Water (NADW), and returns southward along the eastern continental margin. The computed velocities and directions confirm that the WBUC in this area is a contour-following current.

A layer of cold isothermal water 20–170 m thick was found on the bottom over much of the section at depths ranging from 3800 to 5400 m. In some locations the layer was capped by a comparatively steep thermal gradient. The higher AABW content of this homogeneous stratum may be a result of the confluence of NADW and AABW. The possibility that a lower turbulent boundary layer exists in the deep ocean, whose velocity field is dependent on bottom roughness, is also examined by applying relationships derived from similar phenomena in the lower atmosphere.

## INTRODUCTION

DIRECT measurement of a southerly flow of abyssal waters in the western North Atlantic Ocean was first made by SWALLOW and WORTHINGTON (1961) with neutrally-buoyant floats and standard hydrographic stations. Since then, others using similar techniques have also demonstrated the existence of this current (VOLKMANN, 1962; BARRETT, 1965). In addition, indirect observations obtained from oriented bottom photographs and sediment distribution indicate a southerly deep flow along the continental margin (HEEZEN, HOLLISTER and RUDDIMAN, 1966; SCHNEIDER, FOX, HOLLISTER, NEEDHAM and HEEZEN, 1967; ROWE and MENZIES, 1968). Now known as the Western Boundary Undercurrent (WBUC), it is also called a ' contour current ' (HEEZEN, HOLLISTER and RUDDIMAN, 1966) since it tends to flow parallel to the topographic isobaths of the continental margin. Its southerly extent has not been fully investigated although oriented bottom photographs suggest a southerly flow of 1–3 cm $sec^{-1}$ at 12°N on the Antilles Outer Ridge (MCCOY, 1969).

South of 35°N the continental slope is separated from the shelf by the broad Blake Plateau. Near 33°N the southeast trend of the Blake–Bahama Outer Ridge should divert part of the contour following current from its southerly course to a more southeasterly direction (HEEZEN, HOLLISTER and RUDDIMAN, 1966).

*Lamont–Doherty Geological Observatory Contribution No. 1591.
†Lamont–Doherty Geological Observatory of Columbia University, Palisades, New York 10964.
‡U.S. Naval Oceanographic Office, GOFAR, Chesapeake Beach, Maryland 20732.

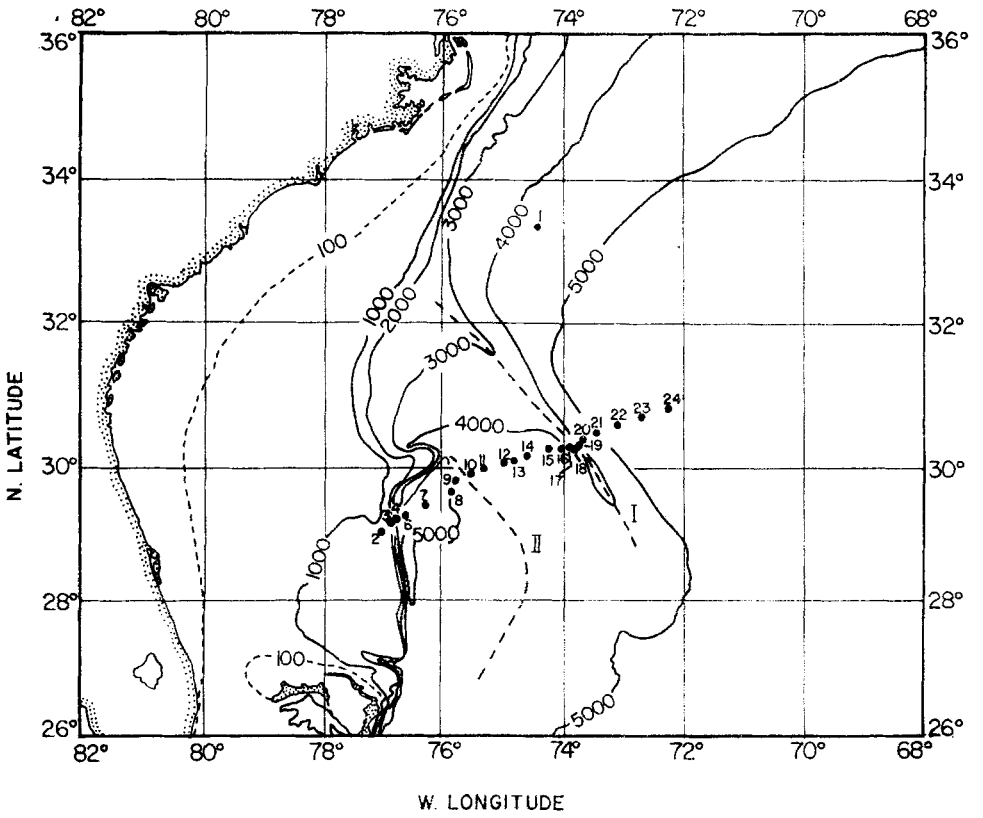


Fig. 1. Location of USNS *James T. Gilliss* Cruise 85 STD stations, May–June, 1968. Blake–Bahama Outer Ridge crests shown by hatched lines labelled I (primary) and II (secondary).

To further examine the WBUC in this region, a closely-spaced series of 22 hydrographic stations was taken using a Bissett Berman Model 9006 Salinity/Temperature/Depth (STD) system with a 6000 m full-scale depth sensor. The STD line runs from the Blake Plateau to the Hatteras Abyssal Plain, crossing the Blake–Bahama Abyssal Plain and two crests of the outer ridge: the secondary ridge rising to 4400 m and the primary ridge extending to above 3800 m (Fig. 1). The Blake–Bahama Abyssal Plain has recently (Aug. 18, 1970) become of special interest as the area chosen for the much-publicized dumping of obsolete nerve gas. The supposed location of the dump-site is between Stas. 7 and 8.

## PROCEDURE

The STD data were recorded on both analog charts and in digital format on magnetic tape with the Bissett Berman Digital Data Logger. At each station the STD was lowered at 25–30 m/min until it was below the main thermocline to minimize erroneous salinity excursions caused by the disparity in time constants of the conductivity head and the temperature compensatory elements in the salinity sensor. These excursions become large when the instrument is lowered through a steep temperature gradient. Below the thermocline the lowering rate was increased to a maximum of 100 m/min. A Benthos bottom-finding pinger was attached directly to the STD instrument cage

permitting continuous measurements down to within 10 m of the bottom at most of the stations without risk of damaging the sensors.

Analog and digital recordings were made for both the lowering and raising of the STD. A single scan of the three parameters was recorded on magnetic tape at ~ 0·5 sec intervals. The maximum magnetic tape recording resolution of the 6000 m depth sensor is approximately 0·8 m allowing better than one ' observed level ' of information per meter.

*Accuracy of Gilliss STD data*

The STD is entirely satisfactory within the manufacturer's stated limits of accuracy (salinity ± 0·03‰; temperature ± 0·02°C; depth ± 0·25% full scale; Howe and Tait, 1965); however, this accuracy is lower than that required for significant determination of deep geostrophic velocity and volume transport computations (Gordon, 1967), and individual STD units can be subject to significant variations from the ideal frequency/parameter relationships, to output frequency shifts, and to certain pressure-dependent errors. The necessary increase in accuracy of the STD system can be achieved by comparing STD output with water samples and temperature measurements taken at exactly the same location and time as the STD measurement. This was accomplished with a command-type multiple water sampler (Gerard and Amos, 1968; Niskin, 1968).

*Rosette/STD comparisons*

To quality-control the *Gilliss* data, a 10-bottle Niskin rosette sampler was attached to the STD frame. An attempt was made to cover the entire depth range with evenly spaced samples. The frequency output (monitored on an electronic counter and scanner system and later converted to their respective parameters) of each of the three sensors was recorded at the time a rosette bottle was tripped. The salinity of the water samples was determined with a shipboard induction salinometer. The reversing thermometer data were corrected in the usual manner, but special care was taken to use three thermometers per frame of known performance.

Assuming that the measured salinities of the rosette samples, and the reversing thermometer temperatures and thermometric depths are correct, plots of $\Delta P$ vs. $P_r$ were made, where $P_r$ = parameter value as determined by rosette sample and $\Delta P = P_r - P_{std}$ (the STD parameter value) (Fig. 2).

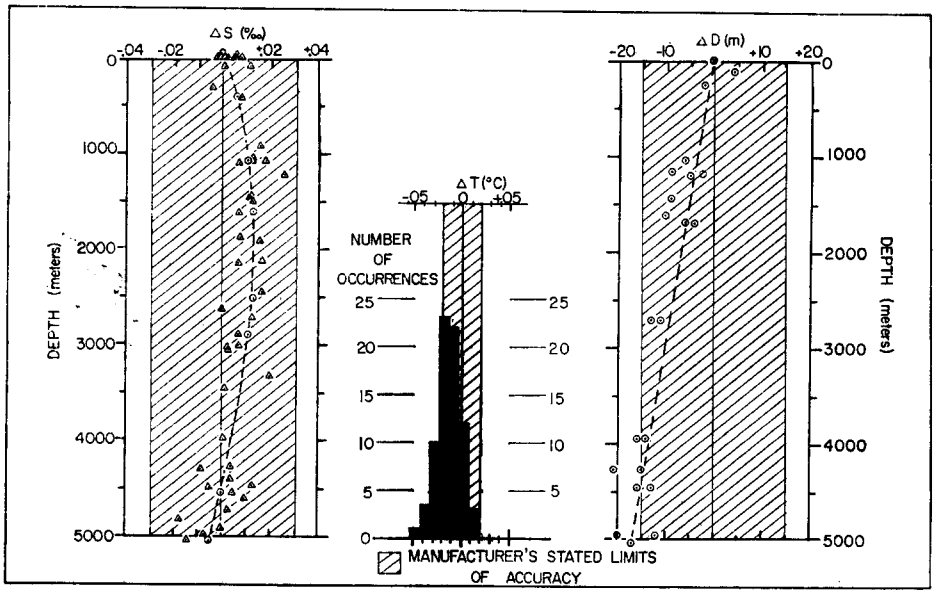


Fig. 2. Difference between standard command sampler measurements and STD output for (a) salinity, plotted as a function of depth; (b) temperature, showing frequency distribution of differences between protected reversing thermometers and STD output; and (c) depth. Hatched lines on (a) and (c) are curves used to correct the STD data.
△ = $\Delta S$ and ⊙ = $\Delta D$ obtained from the command sampler

These plots were examined for obvious shifts and a best-fit curve was computed from the data. The corrections of the STD output were based on this curve. In the case of salinity, a pressure-dependent error was found; a type of error noted previously (AMOS, 1966; JACOBS and AMOS, 1967). Even the small salinity/depth error of the present sensor was obvious when compared with other data (FUGLISTER, 1960; WORTHINGTON and METCALF, 1961; WORTHINGTON and VOLKMANN, 1965) collected in our area.

The bottom depth was measured in three ways: (1) by converting the precision depth recorder (PDR) travel time to meters with MATTHEWS (1939) tables for the speed of sound in sea water; (2) adding the distance of the STD from the bottom, as indicated by a pinger to the deepest STD depth sensor reading; and (3) thermometric depths of rosette thermometers reversed near the bottom (two unprotected and one protected thermometer were attached to the bottom bottle). Bottom depths computed by the two latter methods differed from the first by almost one per cent. This disparity could not be accounted for by recomputing travel time of the PDR impulse, by averaging sound velocity calculated at every level of the actual STD station, or by an average density of the water column computed from the same data in the thermometric depth equation. It may result from the constant relationship between pressure and depth used by the STD manufacturer for the depth sensor (based on an ' average sea water density of 1·025 '). For this paper, bottom depths used in the vertical profiles are those computed by method (2), corrected according to Fig. 2 (C).

*Data processing*

The magnetic tape data were converted to parameter values with the manufacturer's straight-line frequency/parameter relationships. Temperature, depth and salinity corrections were applied (Fig. 2). No attempt was made to correct the salinity data for spike errors introduced by the temperature compensating circuitry. The manufacturer's suggested correction for these errors in salinity cannot be applied without knowing the temperature coefficient of conductivity for different salinities (PINGREE, 1969). Exact lowering speed of the instrument package and effects of distance between the compensating sensor elements and the conductivity sensor (GAUL, 1968) also affect the validity of this correction. Dynamic computations are based on interpolated standard level data from the downtrace of each station, which were visually examined for such erroneous excursions before being accepted.

## *Water characteristics*

The upper 1000 m of the section (Figs. 3, 4) have the strong stratification typical of this subtropical region. In the upper 100 m there is a secondary thermocline with a temperature range of 19°–25°C and a main thermocline from 500–1000 m with temperature ranging from 6° to 16°C. Between them is a more homogeneous layer which, from the temperature/salinity relation, appears to be part of the ' 18°C water ' (WORTHINGTON, 1959). The main halocline (Fig. 4) is coincident with the thermocline.

Potential temperature ($^{\circ}\Theta$) (Fig. 5) was calculated for the section below 2500 m to delineate the structure of the deep and bottom water. The deep isotherms ($^{\circ}\Theta$) tend to parallel the bottom topography, particularly across the Blake-Bahama Outer Ridge, whose influence on these isotherms can be seen as shallow as 2500 m. The strong horizontal temperature gradient near the primary ridge is similar to that observed on the continental margin of the eastern United States (SWALLOW and WORTHINGTON, 1961) and the continental slope off Argentina (WÜST, 1933), and must be indicative of strong currents.

The area of the $\Theta/S$ curve (Fig. 6) centered at about 3·5°C and at approximately 2000 m where the temperature drops with little change in salinity, can be traced to Labrador Sea water (salinity minimum at 3·5°$\Theta$; WORTHINGTON and METCALF, 1961). The inflection point below this layer can be attributed to the influence of the middle North Atlantic Deep Water (WÜST, 1936), and the change in slope at 1·9°$\Theta$ and

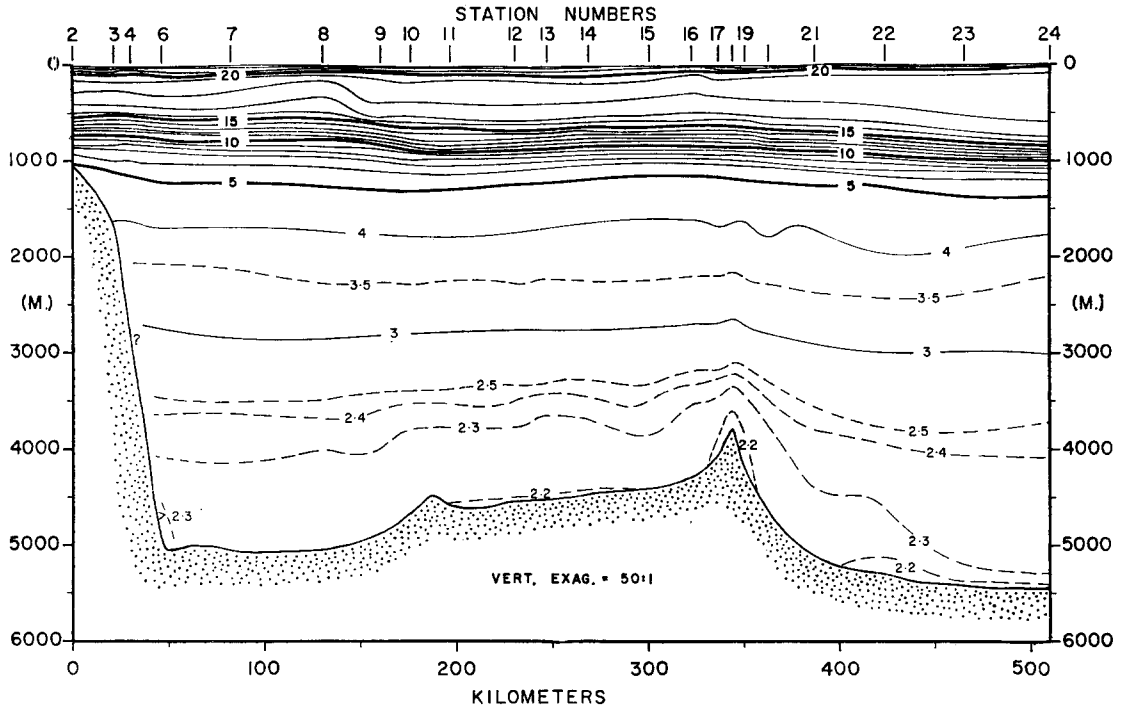


Fig. 3. *In-situ* temperature profile, *Gilliss-85*, Stas. 2–24.

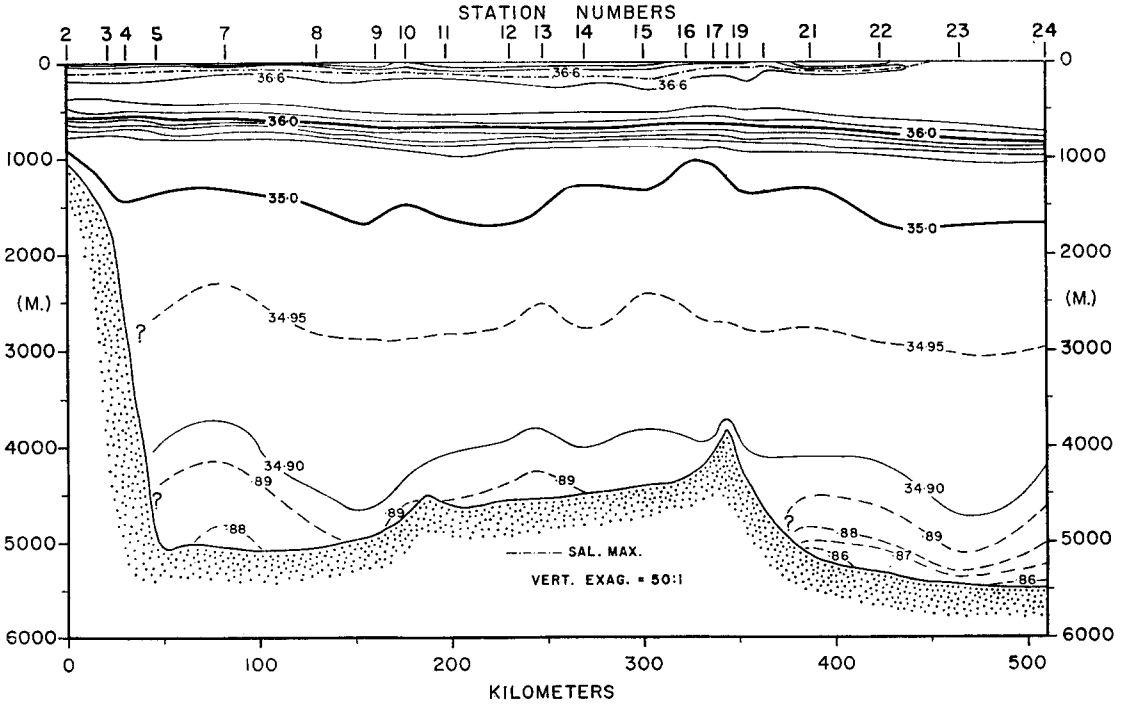


Fig. 4. Salinity profile, *Gilliss-85*, Stas. 2–24.

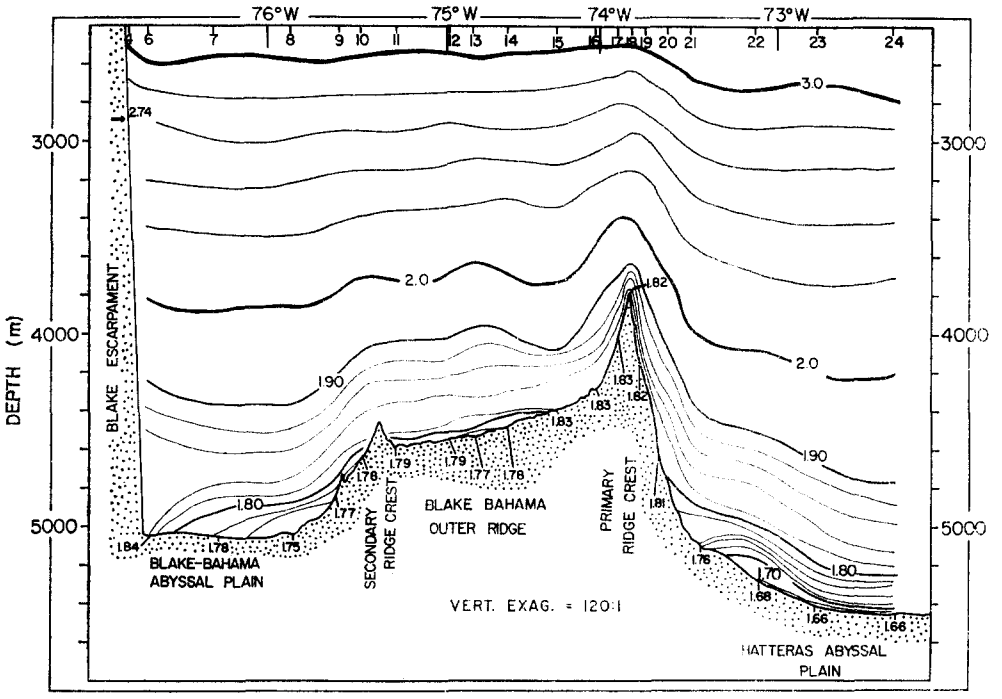


Fig. 5. Potential temperature profile, *Gilliss-85*, Stas. 4–24 below 2400 m. Numbers at base of each station location are deepest potential temperature values.

$S = 34{\cdot}9‰$ is the transition point between lower North Atlantic Deep Water and Antarctic Bottom Water (WÜST, 1933). A measure of the reliability of this STD data is its revelation of the potential density minimum ('potential' with respect to the sea surface reference) typical of this area (Fig. 7) and associated with the transition between NADW and AABW (LYNN and REID, 1968).

The lower and middle North Atlantic Deep Water masses (WÜST, 1936) make up the body of the deep water in the Blake–Bahama area. No influence of upper NADW can be detected. The AABW content at the bottom varies from 12% to 20% using WÜST's (1933) percentages (Figs. 7 and 8). The highest percentages of AABW (15–20%) are grouped in three locations on the bottom: in the Blake–Bahama Abyssal Plain, between the secondary and primary ridges, and in the Hatteras Abyssal Plain.

*Geostrophic velocity determinations*

Geostrophic velocities relative to zero at the surface (Fig. 9a) were determined by the method described by DEFANT (1961, p. 486). Because of the continuous nature of the 'observed' data, standard level intervals were closer than those normally used. In addition, the interpolation errors for these standard levels were minimal since the observed levels were seldom greater than 2 m apart.

The critical problem of selecting a reference level without aid of direct current measurements was approached in two ways:

1. STOMMEL (1956) gave a numerical procedure for determining the level of no

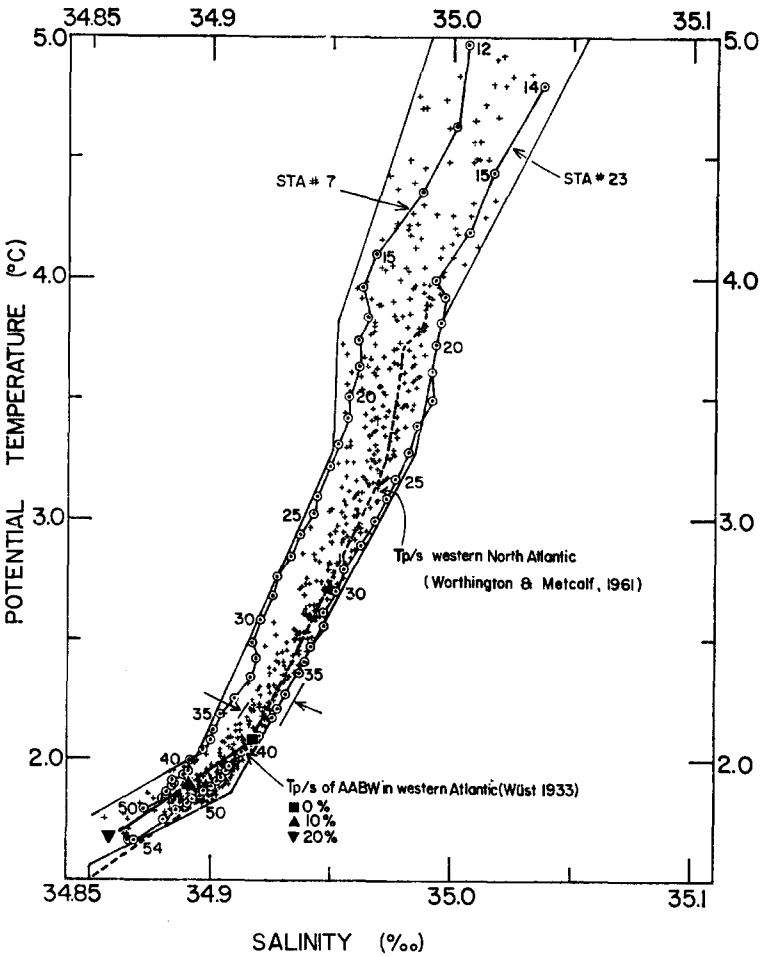


Fig. 6. Potential temperature–salinity relationship, *Gilliss-85*, Stas. 1, 4–24, plotted at 100-m intervals (crosses) for values below 5°$\Theta$. The cloud of points is enclosed by an envelope delineating the maximum spread of these measurements. The composite $\Theta/S$ curve of WORTHINGTON and METCALF (1961) is indicated by a dashed line. Stas. 7 and 23 are indicated by a solid line joining circled points (depths in hectometers). Opposing arrows indicate maximum spread of VOLKMANN's (1962) observations.

meridional motion. Rearranging Stommel's equation 11, the level of no meridional motion is found when:

$$\phi(z) \cdot B = \int_{-B}^{O} \phi(z)\,dz - \frac{f}{\beta} \cdot F(o) \qquad (1)$$

where $B$ = bottom depth
$F(o)$ = net convergence of the Ekman wind-driven layer (MONTGOMERY, 1936)
$f$ = Coriolis parameter
$\beta$ = change of $f$ with latitude

and $\phi(z) = -\frac{g}{f} \cdot \int_{-B}^{z} \frac{\partial \rho}{\partial x}\,dz$

which can be approximated by:

$$-\frac{g}{f}\sum\left[\left(\frac{\Delta\rho}{\Delta L}\right)_{B+z}+\left(\frac{\Delta\rho}{\Delta L}\right)_{B+z+\Delta z}\right]\Delta z$$

where $g$ = acceleration due to gravity,

$\left(\frac{\Delta\rho}{\Delta L}\right)_{B+z}$ = change in density between two stations, $\Delta L$ apart at the standard level $B+z$

and $\left(\frac{\Delta\rho}{\Delta L}\right)_{B+z+\Delta z}$ = the density change at the next standard level above the $B+z$ level.

The summation process begins at the bottom.

For this paper, $F(o)$ was taken from MONTGOMERY's (1936, Fig. 1) diagram, where drift current convergence is given for the North Atlantic in July. (The *Gilliss* section was taken in May and June.)

2. DEFANT's (1961, p. 494) method for determining the level of zero geostrophic velocity was also applied and compared to Stommel's method (Fig. 9b). The arrows on each relative velocity profile in Fig. 9a denote layers of little or no

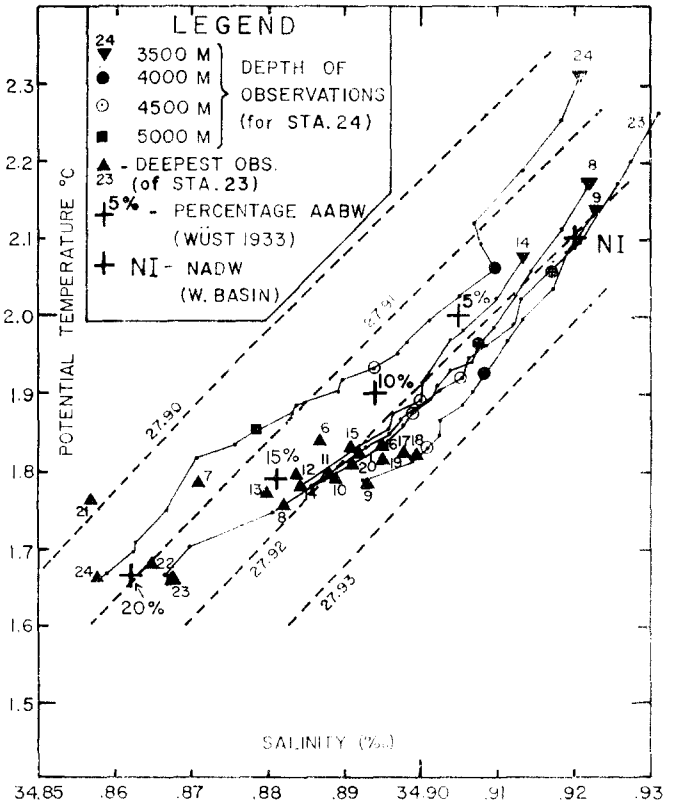


Fig. 7. Expanded potential temperature–salinity diagram, showing deepest observations at *Gilliss* Stas. 1, 4–24 and selected stations below 3500 m to illustrate potential density minimum. The hatched lines of equal potential density, $\sigma\theta$, are in g/l., where $\sigma\theta = 10^3(\rho\theta - 1)$.

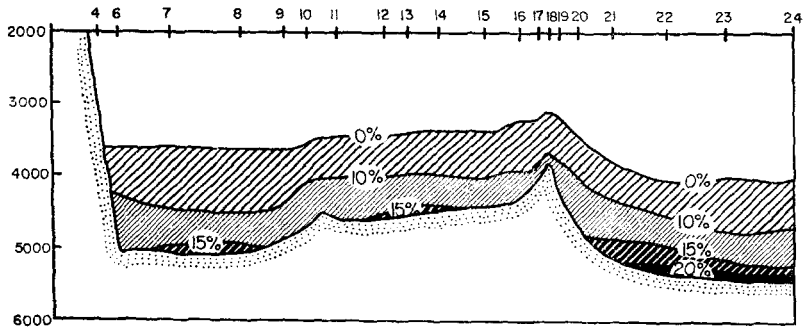


Fig. 8. Profile of Antarctic Bottom Water content of *Gilliss* Stas. 6–24.

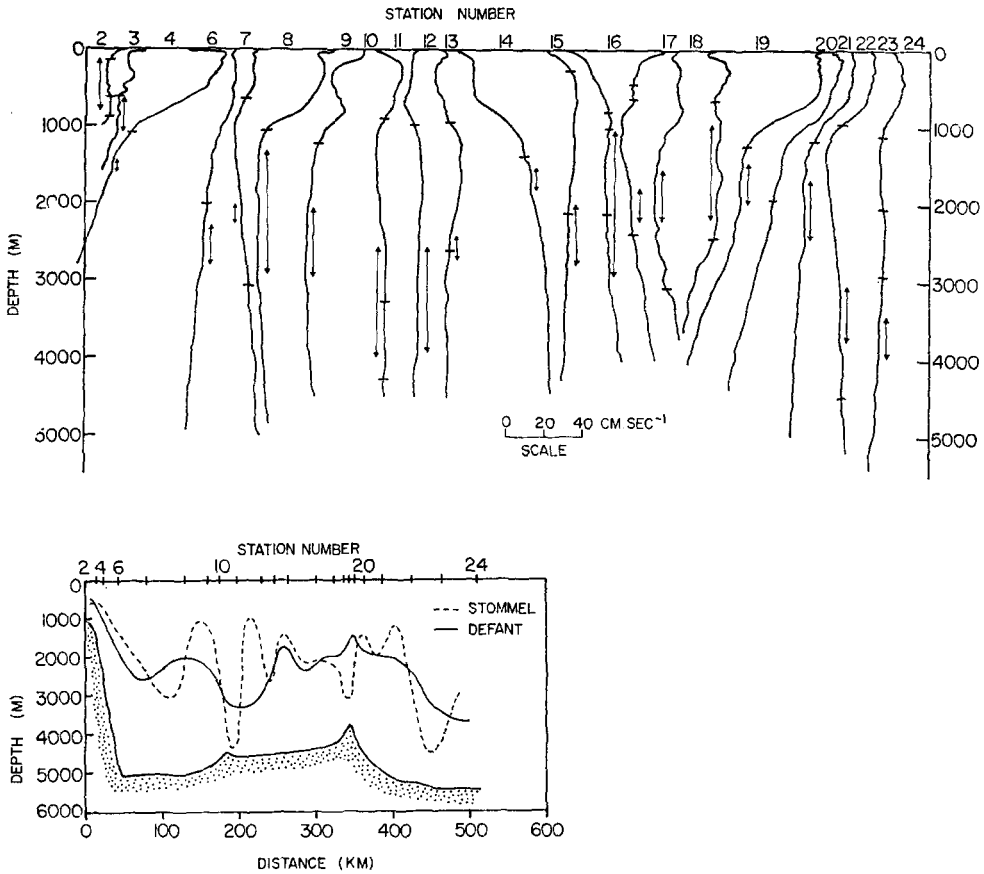


Fig. 9. (a) Geostrophic velocity profiles between station pairs numbered on top axis. Vertical arrows indicate Defant reference zones. Horizontal lines intersect profiles at level(s) of no meridional motion (from STOMMEL, 1956). (b) Location of zero velocity reference levels for the *Gilliss* section.

velocity gradient. The zero velocity reference level is determined as lying anywhere in the layer of no velocity gradient. By examining the family of curves for a section the most probable reference level for each profile can be determined.

While the basic velocity cross-section does not change noticeably with the change of reference level, the volume transport changes enormously. Stommel's method gives a net southerly transport of $3{\cdot}8 \times 10^6$ m$^3$ sec$^{-1}$, while Defant's indicates a northerly net transport of $31{\cdot}4 \times 10^6$ m$^3$ sec$^{-1}$. Below both reference levels, there is a net southerly flow (the Western Boundary Undercurrent): $39{\cdot}8 \times 10^6$ m$^3$ sec$^{-1}$ (Stommel), and $19{\cdot}2 \times 10^6$ m$^3$ sec$^{-1}$ (Defant). Most of the difference comes from station pairs where Stommel's level is shallower than Defant's and large areas of negative (southerly) flow are indicated by Stommel's method, while these areas are close to zero or positive by the Defant reference level.

We have chosen to use the Defant level of no motion because volume transports more closely agree with the historical water budget data of the area. However, the disparity between the two procedures clearly points out the need for a reference based on direct current measurements in conjunction with a hydrographic section such as the present one.

The velocity profile (Fig. 10) is shown in box diagram form rather than a contoured profile, since the calculated velocities are average values between station pairs. Over a sloping ocean floor the deepest calculated velocity is considered to remain constant to the bottom. Three areas of high bottom velocities are found across the section: (1) on the Blake Escarpment, (2) and (3) on both sides of the primary outer ridge. On the eastern flank of the ridge, where the main body of the WBUC might be expected to flow bottom velocities are approximately 25 cm sec$^{-1}$.

Other bottom velocities of similar magnitude have been observed in the western North Atlantic Basin: 17 cm sec$^{-1}$ for 16 hr at 5200 m (KNAUSS, 1965, using a current meter); 20 cm sec$^{-1}$ at 3300 m, 17 cm sec$^{-1}$ at 3500 m (SWALLOW and WORTHINGTON, 1961); 15 cm sec$^{-1}$ at 4000 m (VOLKMANN, 1962); 10 cm sec$^{-1}$ at 3000 m (BARRETT, 1965); the last four measurements being geostrophic velocities computed using Swallow float data for reference.

The deepest geostrophic velocities perpendicular to the *Gilliss* profile agree in principle with the relative current speed and directions deduced from oriented bottom photographs (Fig. 11) lending support to the hypothesis that the Western Boundary Undercurrent is a 'contour' current (HEEZEN, HOLLISTER and RUDDIMAN, 1966). Reversals in direction are found on either side of both crests of the ridge system. On opposite flanks of the primary ridge where the bottom currents are swiftest, the very similar characteristics of water (Fig. 7) flowing in opposing directions add credence to this proposal.

*Table* 1. *Volume transports computed for the* Gilliss *section.*

| *Transport* | *Dir.* | *Provinces* | | | |
|---|---|---|---|---|---|
| | | 1 | 2 | 3 | *Totals* |
| *Surface* | N (+) | 39·0 | 12·5 | 32·0 | 83·5 |
| *to* | S (−) | 12·1 | 12·4 | 25·2 | 52·1 |
| *bottom* | Net | + 26·9 | + 0·1 | + 6·8 | + 31·4 |
| *Below* | N (+) | 9·1 | 6·9 | 0·6 | 16·6 |
| *reference* | S (−) | 9·6 | 3·7 | 22·5 | 35·8 |
| *level* | Net | − 0·5 | + 3·2 | − 21·9 | − 19·2 |

Provinces: 1, edge of Blake Escarpment to secondary ridge crest; 2, between two ridge crests; 3, east of primary ridge crest.

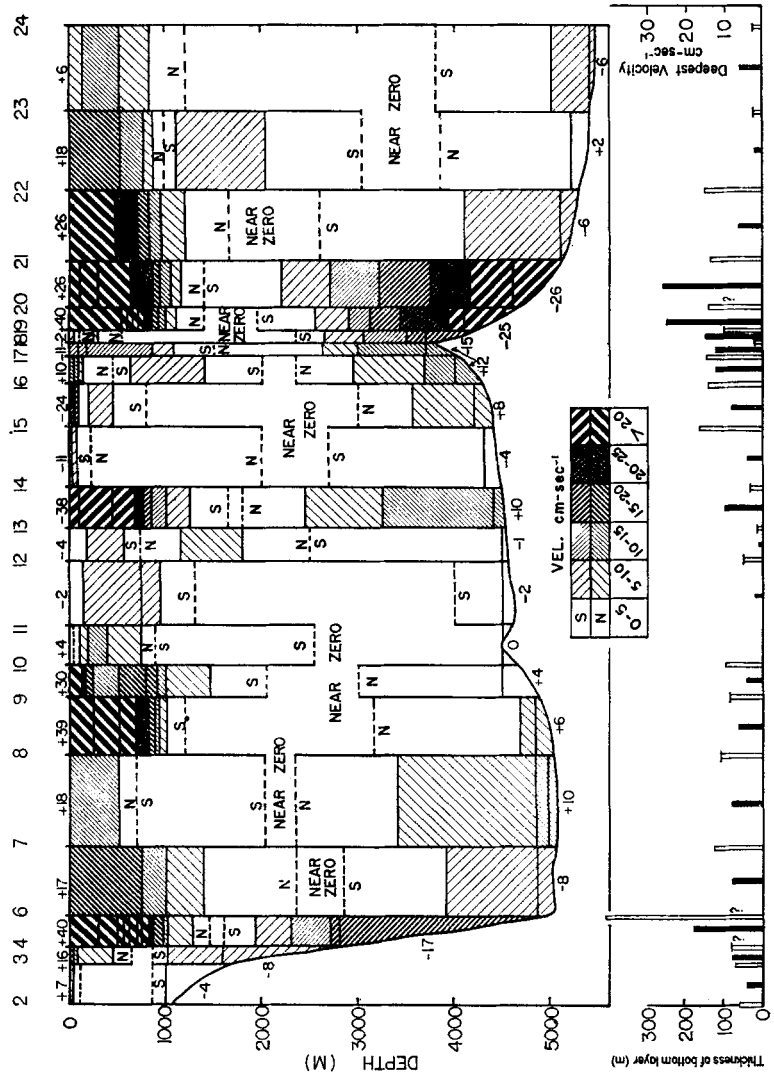


Fig. 10. Velocity field of *Gilliss* section. The numbers at the surface and bottom between each station pair show the magnitude (in cm sec$^{-1}$) and direction (positive = flow to the north; negative = flow to the south) of the surface and deepest geostrophic velocities. Deepest velocities (black bars) and thickness of bottom isothermal layer (open bars) are plotted at corresponding locations along bottom axis. Horizontal line across top of open bar indicates where a steep thermal gradient is found above the layer. Question mark indicates layer of uncertain thickness.

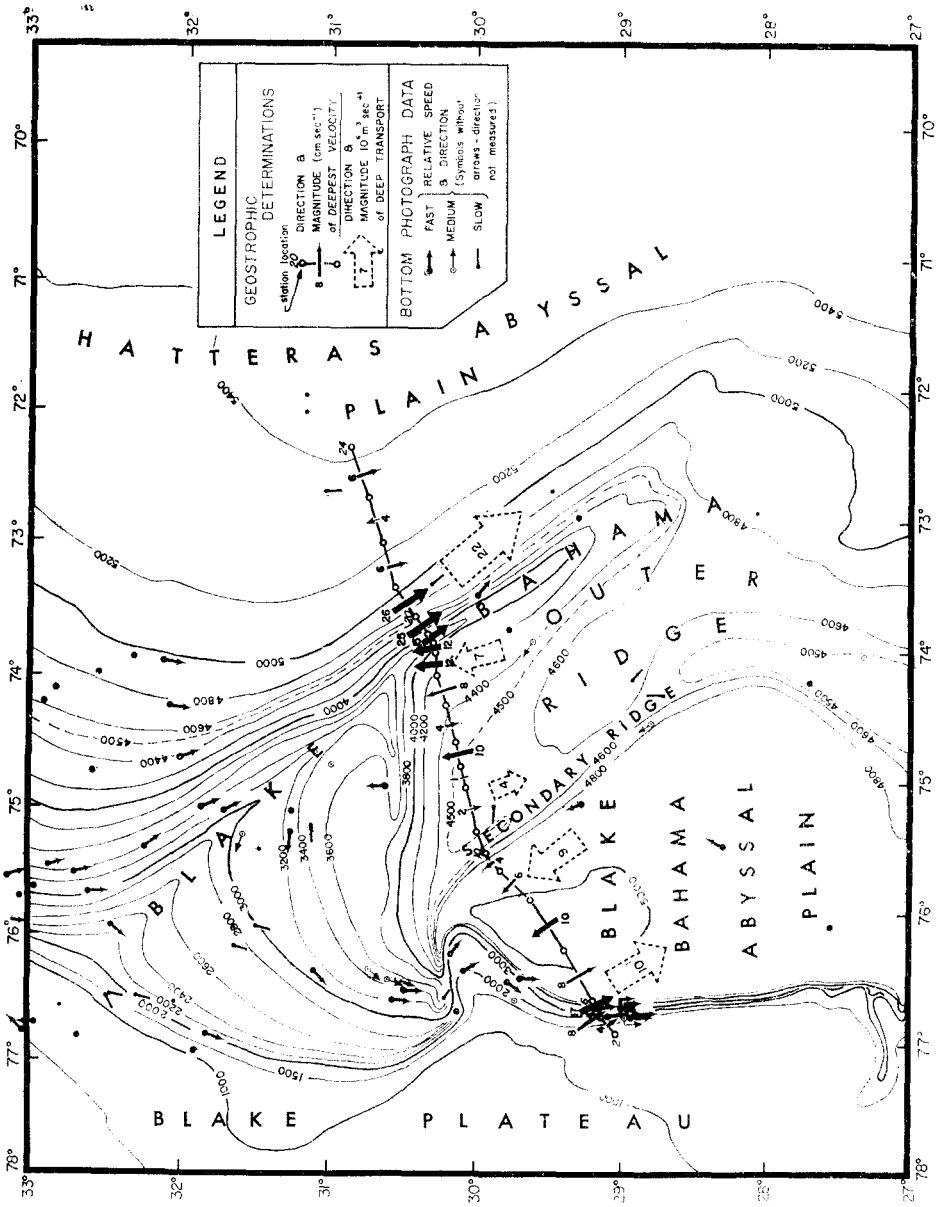


Fig. 11. Deepest geostrophic velocities compared to bottom photograph data in the Blake–Bahama region.

*Volume transports*

The volume transports (Table 1) have been determined for three topographic provinces (see Fig. 11): (1) from the Blake Escarpment to the secondary outer ridge; (2) between the secondary and primary Blake–Bahama outer ridges; and (3) east of the Outer Ridge.

The bulk of the WBUC continues to flow south along the eastern flank of the primary ridge as might be expected from a contour-following current, due to regional topography. In the depression between the two crests the northerly transport exceeds the southerly. In fact, from the main ridge crest to the Blake Escarpment the northerly deep transport is $7 + 9 = 16 \times 10^6$ m$^3$ sec$^{-1}$ and the southerly $10 + 4 = 14 \times 10^6$ m$^3$ sec$^{-1}$, leaving $2 \times 10^6$ m$^3$ sec$^{-1}$ to the north to be accounted for. This is most likely an error in transport values or perhaps a loss of upward flow across the reference level (STOMMEL, 1956; ROBINSON and STOMMEL, 1959). In the Blake–Bahama Basin, west of the secondary ridge, where the sea floor is deeper than that to the east of the ridge, the northerly and southerly deep transports are $10 \times 10^6$ m$^3$ sec$^{-1}$ and $9 \times 10^6$ m$^3$ sec$^{-1}$, respectively. The AABW content of Stas. 7 and 8 (Fig. 7), and the bottom potential temperature distribution indicate that AABW enters the Blake–Bahama Basin as well as the Hatteras Abyssal Plain (WÜST, 1933; HEEZEN and FEDUKOWICZ, 1961), while current directions indicate that a cyclonic circulation pattern occurs within this basin (Fig. 11). Bottom velocities of up to 10 cm/sec could be an important factor in determining the dispersal of any nerve gas leaking from containers now on the bottom there.

AABW contributes significantly to the main southerly flow of the WBUC east of the primary Outer Ridge (Fig. 8). This would necessitate a return flow of AABW that enters the North American Basin (HEEZEN, SCHNEIDER and PILKEY, 1966). A western deflection of AABW probably occurs north of 35°N in the province of the lower continental rise hills that separates the Hatteras and Sohm Abyssal plains. The flow of AABW is considerably weakened at these high northern latitudes, and the minor relief of the abyssal hills may be sufficient to deflect the current to the west and south. Entrainment by the swifter WBUC, composed mainly of NADW at this latitude, could cause this water mass to increase in velocity and become a component of the Western Boundary Undercurrent (Fig. 12). LAPPO (1963), using *Mikhail Lomonosov*, *Crawford* and *Hidalgo* data, shows (his Fig. 1c) a cyclonic circulation in the western North Atlantic Basin below 4000 m.

Previous estimates of the transport of the WBUC (Fig. 12) vary widely and differ from the present computations. Several reasons for these differences may be cited:

1. The determination of an eastern (or southern) boundary is not definite in any of the sections. The assumption has been made that at some point to the east (or south) the current velocity is zero at the bottom. Recently, ROWE and MENZIES (1968) suggested that the WBUC may be fragmented and separated by areas of tranquil bottom resulting in possible underestimated volume transports in previous works.

2. The horizontal extent and the maximum depth of the different sections vary considerably; e.g. the BARRETT (1965) sections extend 100 km out to the 3500 m isobath, while VOLKMANN (1962) includes an area 280 km horizontally out to the 4800 m isobath. Thus, Barrett does not include large areas through which the WBUC may be flowing in computing his transport estimates.

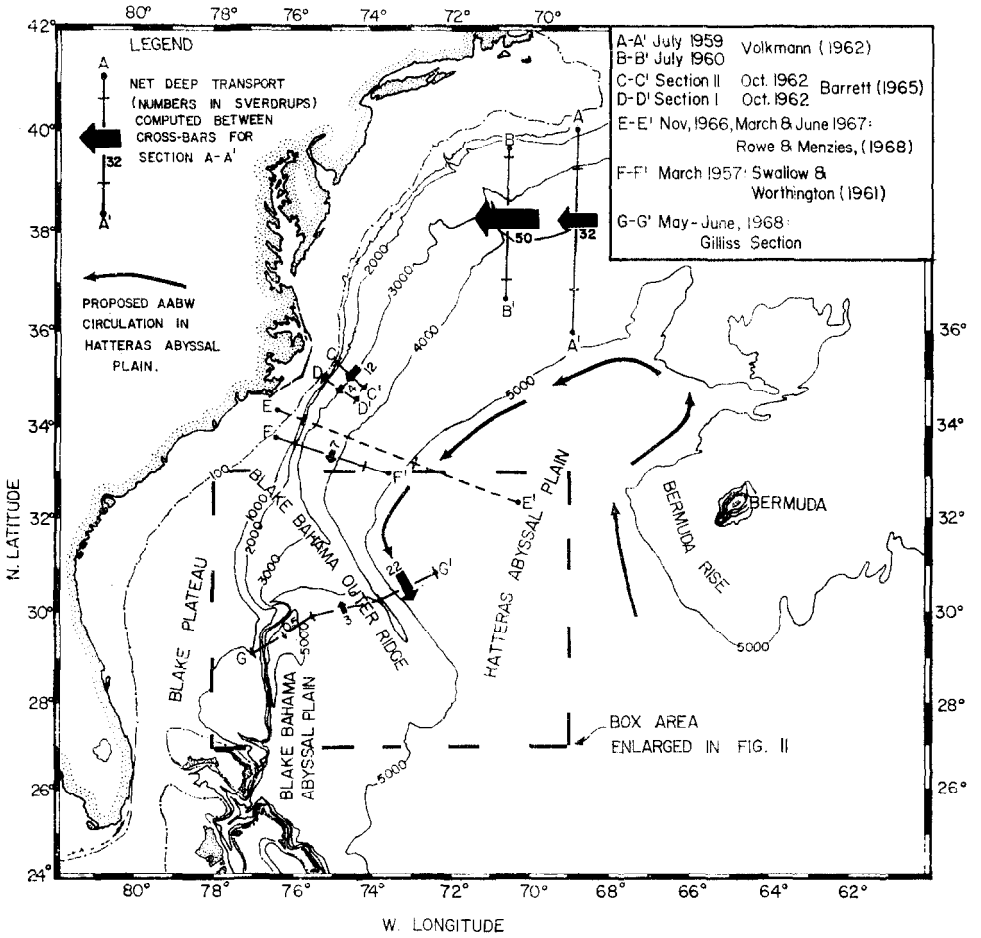


Fig. 12. Transport of the Western Boundary Undercurrent compared to previous determinations.

3. The Volkmann sections show no layer of zero velocity (except directly under the Gulf Stream), and an arbitrary cut-off at 1400 m has been made in determining transports. Volkmann, assuming uniform velocity of 10 cm $sec^{-1}$ above 1400 m, shows that, if the WBUC extended to the surface south of Cape Cod, the transport would be 94 $\times$ $10^6$ $m^3$ $sec^{-1}$ for the 1959 section.

4. Swallow and Worthington, Barrett and Volkmann all used neutrally-buoyant floats to find a reference level. The methods of extending the reference level to station pairs where direct observations were not available were different in these sections.

5. Measurements cannot be considered synoptic, as they were taken from March (Swallow and Worthington) to October (Barrett).

In considering the transport above the reference level for the entire *Gilliss* section, we find 50 $\times$ $10^6$ $m^3$ $sec^{-1}$ flowing to the north. If this represents the Antilles current (COSTIN, 1968), we arrive at 82 $\times$ $10^6$ $m^3$ $sec^{-1}$ (adding 32 $\times$ $10^6$ $m^3$ $sec^{-1}$ for the Florida current, from SCHMIDT and RICHARDSON, 1968) for the Gulf Stream. This

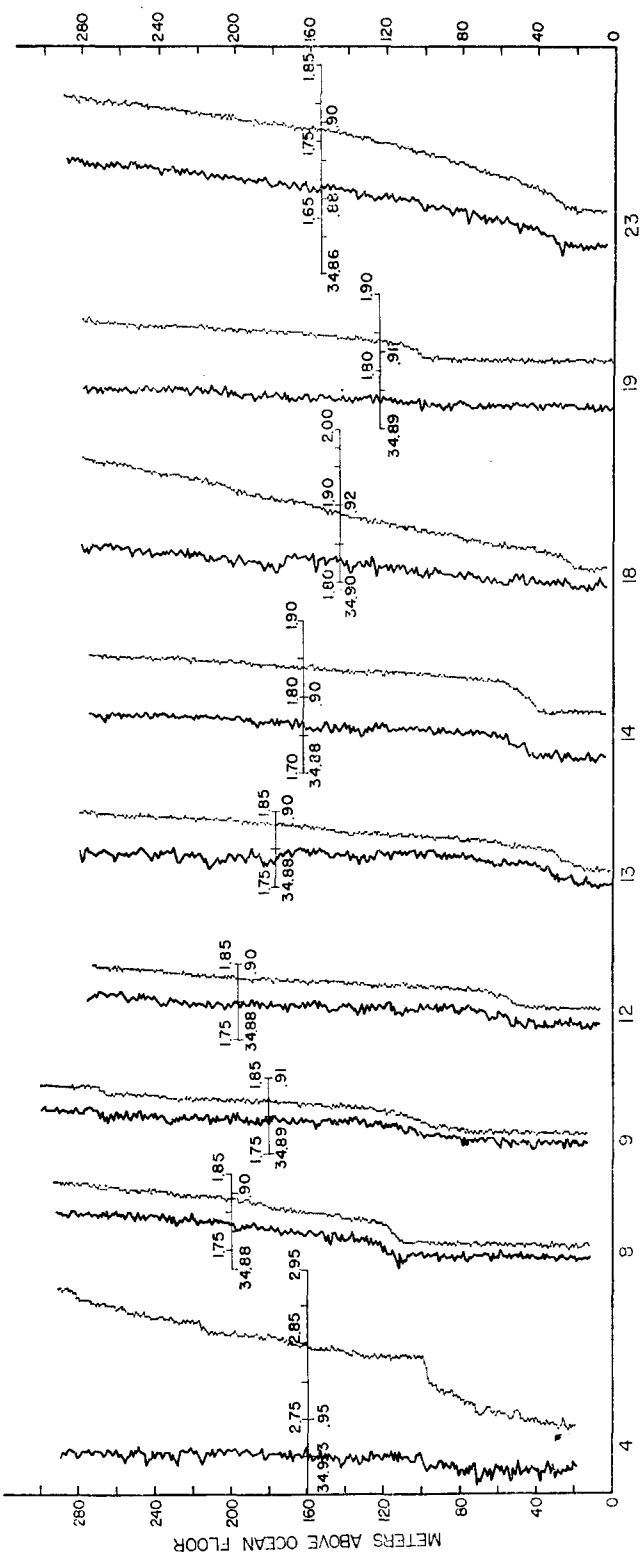


Fig. 13. Expanded bottom STD potential temperature and salinity traces, showing the temperature discontinuity at the bottom. Station numbers on bottom axis. Data plotted from all observed values: temperature shown by light trace, salinity by heavy trace. Distance of trace from bottom axis indicates closest approach of STD to bottom. Individual scales are included for each pair of traces: top scale, potential temperature; bottom, salinity.

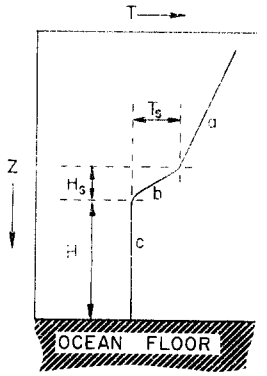


Fig. 14. Schematic structure of the bottom homogeneous layer. Key to Table 2.

*Table 2. Near-bottom thermal gradient measurements.*
(Refer to Fig. 14)

| *Sta. No.* | *$\frac{\partial t}{\partial z}$ (°C × $10^{-3}$ $m^{-1}$) a | b | c | $H_s$ (m) | $H$ (m) | $T_s$ (°C) | $Z$ (m) | *Latitude* |
|---|---|---|---|---|---|---|---|---|
| GI–85–1 | 0·2 | 1·3 | 0 | 16 | 68 | 0·02 | 4377 | 33°N |
| GI–85–8 | 0·4 | 3·1 | 0 | 8 | 110 | 0·03 | 5029 | 30°N |
| GI–85–9 | 0·2 | 1·4 | 0·1 | 14 | 83 | 0·02 | 4639 | 30°N |
| GI–85–12 | 0·2 | 1·4 | 0 | 16 | 49 | 0·02 | 4544 | 30°N |
| GI–85–13 | 0·2 | 1·6 | 0 | 16 | 19 | 0·03 | 4520 | 30°N |
| GI–85–14 | 0·2 | 2·5 | 0 | 17 | 41 | 0·04 | 4459 | 30°N |
| GI–85–18 | 0·4 | 2·9 | 0 | 7 | 24 | 0·03 | 3776 | 30°N |
| GI–85–19 | 0·2 | 1·8 | 0 | 11 | 104 | 0·02 | 4154 | 30°N |
| GI–85–23 | 0·8 | 2·5 | 0·1 | 8 | 25 | 0·02 | 5410 | 31°N |
| GI–85–24 | 0·5 | 3·3 | 0·1 | 9 | 21 | 0·03 | 5444 | 31°N |

*All finite gradients are negative.

compares favorably with the $100 \times 10^6$ $m^3$ $sec^{-1}$ recently estimated by WARREN and VOLKMANN (1968) further north, assuming additional water is entrained in the Gulf Stream north of the *Gilliss* section.

*Bottom isothermal layer*

At several stations a homogeneous layer of relatively cold, fresh water, varying in thickness between 20 and 170 m, was found at the bottom (Figs. 13 and 14 and Table 2). This stratum was separated from the water above by a thin layer in which the thermal gradient was considerably steeper than the normal gradient of the deep water. A similar feature was found at a single *Gilliss* station (No. 1) at 33° 24′N, 74° 24′W, some 300 km to the north of the section under discussion. The temperature and salinity changes near the bottom shown by the STD were verified using the command sampler. Isothermal layers were found at the bottom at most other locations (notably Sta. 6) sampled, but these were not capped by a relatively large temperature gradient. Although the magnitude of this structure is small, it is unusual to find any such changes in the water column at these depths. At Sta. 14, for example, a 0·04°C drop in temperature occurs in 17 m near the bottom, while above that the same change takes place in about 600 m. Two explanations of this phenomenon are:

1. A homogeneous water mass is flowing beneath another water mass for a considerable distance, and intermixing of these two masses is restricted by the stable layer which forms their mutual boundary.

2. A turbulent boundary exists at the bottom, causing a mixed (homogeneous) layer whose thickness is dependent upon the roughness of the bottom topography and the magnitude of the current. A similar layer is formed in the lower atmosphere, where the velocity profile within the boundary layer can be shown to be a function of surface roughness and layer thickness (ROSSBY and MONTGOMERY, 1935).

## 1. *Bottom water mass*

A homogeneous layer was found at the bottom at every deep station although it was not always capped by a stable layer. The large area and different types of bottom terrain over which this stratum was detected indicate that it may be an extensive feature in the western North Atlantic Basin. Such microstructure could have been previously overlooked due to the paucity of deep, continuous measurements in the area.* The homogeneous layer has more AABW characteristics (low temperature and salinity) than the water directly above. With the exception of Stas. 18 and 19 on the primary Outer Ridge, the mixed layers that have a distinct upper boundary are found in the depressions crossed by the section (Fig. 8) where water of greatest AABW content is found. However, the top of the mixed layer does not represent a transition between AABW and NADW. AABW influence is seen up to 1000 m above the bottom in the entire deep portion of the section (Fig. 8). The layer may be a product of the proposed confluence of AABW and NADW after recirculation in the western North Atlantic Basin. Mixing with the water above is retarded by the relatively stable cap and thus it maintains its identity for relatively long distances downstream of the confluence.

High thermal gradients and isothermal layers close to the bottom have been found in the Atlantic (GERARD, LANGSETH and EWING, 1962) and Denmark Strait (LACHENBRUCH and MARSHALL, 1968) using a heat-flow probe (thermograd) attached to deep-sea coring apparatus.

Another deep-ocean phenomenon associated with bottom circulation is the striking increase in suspended matter (the nepheloid zone) in the water towards the bottom (EWING and THORNDIKE, 1965; THORNDIKE and EWING, 1967). Light-scattering measurements on the Blake–Bahama and Antilles Outer Ridges occasionally show a thin, clear layer on the bottom below the normally sediment-laden nepheloid zone (EITTREIM, EWING and THORNDIKE, 1969). According to these authors, the nepheloid layer of Sta. C11-196† (VEMA Gap) is associated with the Antarctic Bottom Water and is less intense than at nearby stations to the southwest, due to the AABW having deposited much of its sedimentary load by the time it reaches that latitude. The remarkably clear, thin bottom layer of Sta. C11-195 (Antilles Outer Ridge) and similar, but less pronounced, layers of Stas. C11-201, 203, 204 (Blake–Bahama Outer Ridge) may then be water of higher AABW percentage after it has been recirculated and may be related to the cold layers under discussion.

*Even using the STD, some of the thinner layers would have been missed if the bottom-finding pinger had not been used, due to the depth discrepancy mentioned previously.

†R/V *Conrad*, Cruise 11, nephelometer stations.

2. *Turbulent boundary layer*

The ROSSBY and MONTGOMERY (1935) theory attempts to explain the lower turbulent boundary layer in the atmosphere with application to the ocean. At the time of the Rossby–Montgomery paper, strong near-bottom currents in the deep ocean had not been discovered, but they state that their treatment can be applied to the ocean as well as the atmosphere.

The equation governing the thickness of the lower boundary layer (homogeneous layer) is given by:

$$H = 246 \cdot \frac{W_a}{\text{Sin } L \cdot \log\left(\frac{z_a + z_o}{z_o}\right)}$$

(equation (33) ROSSBY and MONTGOMERY, 1935)

where $z_o$ is the roughness coefficient and is related to the actual relief by the empirical equation $z_o = \epsilon/30$ of PRANDTL (1932) ($\epsilon$ = actual relief).

$W_a$ is the velocity at height $z_a$ from the bottom and $L$ is the latitude.

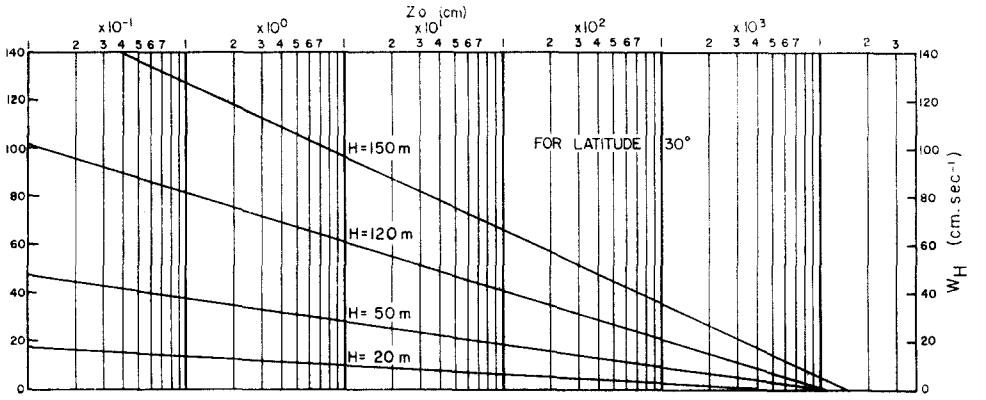


Fig. 15. Velocity at top of turbulent boundary layer ($W_H$) as a function of bottom roughness parameter ($z_o$) for layers of different height ($H$) at latitude = 30°.

A graphic representation (Fig. 15) of the above equation, substituting $W_H$ (velocity at top of layer $H$-meters thick) for $W_a$ shows that to obtain a realistic $Z_o$ (assuming the PRANDTL (1932) relation is valid), either $W_H$ should be much greater than the computed geostrophic velocities or $H$ smaller than observed here. $Z_o$ values computed for the *Gilliss* stations (Table 3) are orders of magnitude larger than those found at land surfaces in ROSSBY and MONTGOMERY (1935).

Several problems arise in using geostrophic velocities as an approximation of $W_H$: geostrophic velocities are computed between station pairs, while the bottom layer is observed at the station locations. We can either interpolate the height of the bottom layer to the center position between station pairs or interpolate the velocity to the location of the observed layer. The former seems unrealistic, as a layer is not found at all station locations and the latter introduces problems where adjacent velocity directions are opposite and interpolation produces close to zero velocity at the station location. The latter method was used for Table 3. A sloping ocean bottom between many stations introduces further uncertainty in the value of $W_H$ used here.

*Table 3. $z_0$ calculations compared to qualitative bottom roughness estimates for* Gilliss *stations.*

| *Sta. No.* | $W_H$* cm sec$^{-1}$ (interpolated) | *H* (m) (observed) | *Depth of $W_H$ calc.* (m) | *Bottom depth* (m) (observed) | *Computed $z_0$* (m) | *Bottom§ type* (observed) |
|---|---|---|---|---|---|---|
| 2 | † | 25 | — | 1069 | — | A |
| 3 | − 7 | 68 | 1420 | 1614 | 31 | C |
| 4‡ | − 11 | 100 | 2032 | 2906? | 40 | C |
| 6 | − 16 | 450 | 3458 | 5013? | 900 | A |
| 7 | + 6 | 135 | 4942 | 5045 | 205 | A |
| 8‡ | + 8 | 110 | 4877 | 5029 | 86 | AB |
| 9‡ | + 5 | 83 | 4670 | 4849 | 85 | B sinusoidal |
| 10 | + 3 | 97 | 4557 | 4641 | 231 | B sinusoidal |
| 11 | − 2 | 0 | 4500 | 4588 | — | B/D sinusoidal & fuzzy hyperbolae |
| 12‡ | − 2 | 49 | 4500 | 4544 | 83 | AB broad undulations |
| 13‡ | + 1 | 19 | 4457 | 4520 | 23 | AB slightly fuzzy |
| 14‡ | + 6 | 41 | 4260 | 4459 | 10 | AB slightly fuzzy |
| 15 | + 2 | 169 | 4243 | 4388 | 1207 | AB slightly fuzzy |
| 16 | + 12 | 140 | 4073 | 4272 | 85 | B fuzzy |
| 17 | + 12 | 145 | 3805 | 4011 | 94 | AB |
| 18‡ | + 2 | 24 | 3700 | 3776 | 15 | AB |
| 19‡ | − 18 | 104 | 3841 | 4154 | 17 | B hyperbolic |
| 20 | − 26 | 146 | 4233 | 4627 | 22 | B small sinusoidal |
| 21 | − 22 | 134 | 4697 | 5073 | 33 | B large hyperbolae |
| 22 | 0 | 153 | 5100 | 5262 | — | AB slightly fuzzy |
| 23‡ | 0 | 25 | 5296 | 5410 | — | A |
| 24 | † | 21 | — | 5444 | — | A |

*Velocity interpolated between adjacent determinations.
†No interpolation possible.
‡Stations shown in Fig. 13.
§Regional echo sounder characteristics with local microtopography: A = coherent; B = hyperbolic echoes; C = incoherent or 'fuzzy'; D = fuzzy hyperbolic echoes.

Qualitative estimates of bottom roughness are made by examining PDR records at the approach to each station. The bottom types (Table 3) are derived from the report of BRYAN and MARKL (1966). Where necessary, combinations of types are given. Quantitative data on local bottom relief are scant. Sand ripples contoured by stereographic photo techniques (SCHULDT, COOK and HALE, 1967) have a relief of approximately 3 cm, which would give a $z_0$ of 0·1 cm. BRYAN and MARKL (1966) give a one meter amplitude for lateral sand waves from bottom photographs ($z_0$ = 3 cm). Recently, ZHITOVSKIY (1968) has reported measuring small mounts 3–5 m high ($z_0$ = 10–17 cm) and 150–200 m in length in 5000 m of water, using a deep-towed transducer. The normal echo sounder record was coherent at the same location and did not show these undulations.

While the turbulent boundary calculations do not seem to support this interpretation of the bottom layer, the following uncertainties must be considered before eliminating this theory: (1) validity of PRANDTL's (1932) $z_0/\epsilon$ relationship in the ocean; (2) difficulty in assessing ocean floor roughness; (3) lack of direct velocity measurements. Table 3 does show a general increase in $H$ with increase in $W_H$ but no satisfactory relationship can be established from this. A graphic representation of deepest geostrophic velocity and thickness of bottom layer is included in Fig. 10. LACHENBRUCH and MARSHALL (1968) consider that turbulent mixing caused by bottom effects on deep currents produces the layers in the Denmark Strait, some of

which they find to have a horizontal extent of > 150 km. Using their assumption that turbulent mixing will not be suppressed by density stratification if the Richardson number is $< \frac{1}{4}$, velocities of 4–10 cm/sec are computed for a 150 m thick homogeneous layer and agree much closer with the geostrophic velocities than with the Rossby–Montgomery calculations. These values are lower than those calculated for the Denmark Strait due to the smaller potential temperature gradient of the deep water in the Blake–Bahama region.

*Acknowledgements*—Acknowledgement is due to Messrs. J. CASON, W. JAHNS, J. FREITAG of Nav-Oceano's Global Ocean Floor Analysis (GOFAR) program and K. GIROUARD of Lamont–Doherty Geological Observatory for their shipboard assistance, and to the officers and crew of the USNS *James T. Gilliss* for their excellent assistance with over-the-side activities. Special acknowledgement is due to Mr. S. S. JACOBS and Drs. B. C. HEEZEN, R. D. GERARD and M. G. LANGSETH for their critical review of the manuscript and valuable suggestions.

This work was supported in part by the Atomic Energy Commission of the U.S. Government under contract AT(30–1) 2663, and in part by the Office of Naval Research under contract NOOO 14–67–A–0108–0004.

## REFERENCES

AMOS A. F. (1966) Physical oceanographic observations in the Indian Ocean using a continuously-recording *in-situ* salinity, temperature and depth sensor. R/V *R.D. Conrad* Cruise 9, 1965. *Tech. Rep. Lamont Geol Observ. IIOE*, 188 pp. (unpublished manuscript).

BARRETT J. R., JR. (1965) Subsurface currents off Cape Hatteras. *Deep-Sea Res.*, **12**, 173–184.

BRYAN G. M. and R. G. MARKL (1966) Microtopography of the Blake–Bahama region. *Tech. Rep. Columbia Univ.* 8, CU–8–Nobsr 85077, 26 pp. (unpublished manuscript).

COSTIN J. M. (1968) Direct current measurements in the Antilles Current. *J. geophys. Res.*, **73**, 3341–3344.

DEFANT A. (1961) *Physical Oceanography*. Pergamon Press, Vol. I, 729 pp.

EITTREIM S., M. EWING and E. M. THORNDIKE (1969) Suspended matter along the continental margin of the North American Basin. *Deep-Sea Res.*, **16**, 613–624.

EWING M. and E. M. THORNDIKE (1965) Suspended matter in deep ocean water. *Science*, **147**, 1291–1294.

FUGLISTER F. C. (1960) Atlantic Ocean Atlas of temperature and salinity profiles and data from the International Geophysical Year of 1957–1958. *Atlas Ser., Woods Hole Oceanogr. Inst.*, Vol. 1, 209 pp.

GAUL R. D. (1968) Performance analysis of a salinity/temperature/depth system. *IEEE Trans. Geosci. Electron.* GE–6, 185–189.

GERARD R. D. and A. F. AMOS (1968) A surface-actuated multiple sampler. *Mar. Sci. Instrument.*, Plenum Press, **4**, 682–686.

GERARD R. D., M. LANGSETH, JR. and M. EWING (1962) Thermal gradient measurements in the water and bottom sediment of the western Atlantic. *J. geophys. Res.*, **67**, 785–803.

GORDON A. L. (1967) Circulation of the Caribbean Sea. *J. geophys. Res.*, **72**, 6207–6223.

HEEZEN B. C. and W. FEDUKOWICZ (1961) Near-bottom potential temperature map of the North Atlantic (unpublished manuscript).

HEEZEN B. C., C. D. HOLLISTER and W. F. RUDDIMAN (1966) Shaping of the continental rise by deep geostrophic contour currents. *Science*, **152**, 502–508.

HEEZEN B. C., E. D. SCHNEIDER and O. H. PILKEY (1966) Sediment transport by the Antarctic Bottom Current on the Bermuda Rise. *Nature, Lond.*, **211**, 611–612.

HOWE M. R. and R. I. TAIT (1965) An evaluation of an *in-situ* salinity–temperature–depth measuring system. *Mar. Geol.*, **3**, 483–487.

JACOBS S. S. and A. F. AMOS (1967) Physical and chemical hydrographic observations in the southern oceans. USNS *Eltanin* Cruises 22–27. *Tech. Rep. Lamont Geol. Observ.* CU–2663–38, 287 pp. (unpublished manuscript).

KNAUSS J. A. (1965) A technique for measuring deep-ocean currents close to the bottom with an unattached current meter, and some preliminary results. *J. mar. Res.*, **23**, 237–245.

LACHENBRUCH A. H. and B. V. MARSHALL (1968) Heat flow and water temperature fluctuations in Denmark Strait. *J. geophys. Res.*, **73** (18), 5829–5842.

LAPPO S. S. (1963) Deep currents in the North Atlantic Ocean. (In Russian). *Okeanologiia*, **3**, 803–813 (Transl. *Deep-Sea Res.*, **11**, 435–439).

LYNN R. J. and J. L. REID (1968) Characteristics and circulation of deep and abyssal waters. *Deep-Sea Res.*, **15**, 577–598.

MATTHEWS D. J. (1939) *Tables of the velocity of sound in pure water and sea water for use in echo-sounding and sound-ranging*. Hydrographic Dept., Admiralty, London, 52 pp.

MCCOY F. N., JR. (1969) Bottom currents in the western Atlantic Ocean between the Lesser Antilles and the Mid-Atlantic Ridge. *Deep-Sea Res.*, **16**, 179–184.

MONTGOMERY R. B. (1936) On the momentum transfer at the sea surface—III. Transport of surface water due to the wind system over the North Atlantic. *Pap. Phys. Oceanogr. Met.*, **4**, 23–30.

NISKIN S. (1968) A deck command multiple water sampler. *Mar. Sci. Instrument*. Plenum Press, **4**, 19–24.

PINGREE R. D. (1969) Small-scale structure of temperature and salinity near station Cavall. *Deep-Sea Res.*, **16**, 275–295.

PRANDTL L. (1932) Meteorologische Anwendung der Strömungslehre. *Beiträge zur Physik der freien Atmosphäre, Bjerknes-Festschrift*, p. 188.

ROBINSON A. R. and H. STOMMEL (1959) The oceanic thermocline and the associated thermocline circulation. *Tellus*, **11**, 295–308.

ROSSBY C. G. and R. B. MONTGOMERY (1935) The layer of frictional influence in wind and ocean currents. *Pap. Phys. Oceanogr. Met.*, **3**, 1–101.

ROWE G. T. and R. J. MENZIES (1968) Deep bottom currents off the coast of North Carolina. *Deep-Sea Res.*, **15**, 711–719.

SCHMIDT W. J., JR. and W. S. RICHARDSON (1968) On the transport of the Florida Current. *Deep-Sea Res.*, **15**, 679–693.

SCHNEIDER E. D., P. J. FOX, C. D. HOLLISTER, H. D. NEEDHAM and B. C. HEEZEN (1967) Further evidence of contour currents in the western North Atlantic. *Earth Planet. Sci. Lett.*, **2**, 351–359.

SCHULDT M. D., C. E. COOK and B. W. HALE (1967) Photogrammetry applied to photography at the bottom. *Deep Sea Photography* (J. B. HERSEY, editor), *Johns Hopkins Oceanogr. Stud.* **3**, 69–73.

STOMMEL H. (1956) On the determination of the depth of no meridional motion. *Deep-Sea Res.*, **3**, 273–278.

SWALLOW J. C. and L. V. WORTHINGTON (1961) An observation of a deep counter-current in the western North Atlantic. *Deep-Sea Res.*, **8**, 1–19.

THORNDIKE E. M. and M. EWING (1967) Photographic nephelometers for the deep-sea. *Deep Sea Photography* (J. B. HERSEY, editor), *Johns Hopkins Oceanogr. Stud.*, **3**, 113–116.

VOLKMANN G. H. (1962) Deep current observations in the western North Atlantic. *Deep-Sea Res.*, **9**, 493–500.

WARREN B. A. and G. H. VOLKMANN (1968) Measurement of volume transport of the Gulf Stream south of New England. *J. mar. Res.*, **26**, 110–126.

WORTHINGTON L. V. (1959) The 18° water in the Sargasso Sea. *Deep-Sea Res.*, **5**, 297–305.

WORTHINGTON L. V. and M. G. METCALF (1961) The relationship between potential temperature and salinity in deep Atlantic water. *Rapp. Proc. Réun. Cons. perm. int. Explor. Mer.*, **149**, 122–128.

WORTHINGTON L. V. and G. H. VOLKMANN (1965) The volume transport of the Norwegian Sea overflow water in the North Atlantic. *Deep-Sea Res.*, **12**, 667–676.

WÜST G. (1933) Das Bodenwasser und die Gliederung der Atlantischen Tiefsee. *Wiss. Ergebn. dt. atlant. Exped. Meteor 1925–27*, **6** (1) (1), 106 pp. (English Transl. No. 340 by M. Slessers, U.S. Naval Oceanographic Office, 1967).

WÜST G. (1936) Schichtung und Zirkulation des Atlantischen Ozeans. Schnitte und Karten von Temperatur Salzgehalt und Dichte. *Wiss. Ergebn. dt. atlant. Exped. Meteor 1925–27*, **6** Atlas, Teil A & B (Stratosphäre).

ZITHOVSKIY Y. Y. (1968) Measurement of bottom irregularities not previously recorded by echo sounding. (In Russian). *Okeanologiia*, **8**, 759–760 (*AGU Translation:* English ed., April 1969, 607–608).